Development of composite cold-formed steel-rubberised concrete semi-rigid moment-resisting connections.

BAGHERI SABBAGH, A., JAFARIFAR, N., DENIZ, D. and TORABIAN, S.

2022

Development of Composite Cold-Formed Steel-Rubberised Concrete Semi-Rigid Moment-Resisting Connections

Alireza Bagheri Sabbagh[a], Naeimeh Jafarifar[b], Derya Deniz[c], Shahabeddin Torabian[d]

[a] School of Engineering, University of Aberdeen, Scotland, UK, alireza.bsabbagh@abdn.ac.uk

[b] School of Architecture and Built Environment, Robert Gordon University, Scotland, UK, n.jafarifar@rgu.ac.uk

[c] Assistant Professor, Department of Civil Engineering, Ozyegin University, Turkey, derya.deniz@ozyegin.edu.tr

[d] Senior Consulting Engineer, Simpson Gumpertz & Heger, Inc. Washington DC, storabian@sgh.com

[d]Adjunct Associate Research Scientist, Department of Civil and Systems Engineering, Johns Hopkins University, Maryland, Baltimore, USA

Abstract

This paper presents the development of a composite cold-formed steel (CFS)-rubberised concrete (RuC) semi-rigid moment-resisting connection suitable for framed building structures. The connection comprises built-up tubular cold-formed steel beam and column sections connected using side-plate screwed fasteners and infilled with rubberised concrete. A detailed finite element analysis validated against physical tests is employed to model both bare steel and composite beam-to-column connections subjected to lateral and gravity loadings. The governing design limit states are characterized as local buckling in bare steel beams, connection screw shear failure, and side plate plasticity. It is shown that the strength and ductility capacity of composite connections could be increased by up to 1.44 and 3.46 times, respectively, compared with those of the bare steel connections. The connection rigidity of both bare steel and composite connections can be classified as a semi-rigid joint.

Keywords: Cold-formed steel; Moment-resisting connections; Semi-rigid joints.

1. Introduction

In the face of the global climate emergency, more efficient utilisation of the structural components in building structures is of critical importance to reduce the overall usage of materials and wastefulness, whilst improving the structural performance. Lightweight steel framing (LSF) structures are gaining popularity for their offsite construction and ease of fabrication and installation employing self-drilling screw connections [1]. LSF systems can offer savings of 30-50% in total construction time, compared with traditional construction methods [2], with environmental benefits of reduced energy consumption and CO_2 emissions. Typical best-practice LSF systems comprising cold-formed steel (CFS) stud walls and joisted floors are, however, being designed with a

considerable number of underutilised sections. The design of the joisted floors being connected to the stud walls through simply supported connections is generally governed by the mid-span deflection serviceability limit state, leading to relatively heavy flooring joists [3]. Premature local failure limit states have also been identified in the components of the floor-to-wall connections through a recently completed study [4], which can lead to an overly conservative design of the stud sections. Within a recent attempt by the authors [5], a semi-rigid moment-resisting screwed floor-to-wall connection has been developed to address the identified drawbacks and improve the strength utilisation of the LSF members.

In parallel with the stud-wall LSF systems, a framed moment-resisting (MR) type of LSF systems have also been developed by Uang and Sato [6] featuring CFS channel beams bolted to both sides of hollow section columns, with the application limited to single-storey structures. More recently, a rigid moment-resisting CFS beam-to-column connection has been developed by the first author [7-11] through a set of physical tests and finite element (FE) analyses suitable for multi-storey building structures in seismic areas. Fig. 1 shows a schematic view of the developed CFS MR connection featuring double back-to-back folded flange channel beam sections connected to a diamond shape column by means of a bolted through plate connection. The folded flange beam sections are used together with the out-of-plane stiffeners (shown in Fig. 1) to postpone the beam local buckling beyond the yielding moment. Furthermore, it has been shown that the friction-slip mechanism within the bolted connections improves the ductility capacity. These enable a relatively high degree of plasticity to be developed inside the CFS beam, meeting the requirements of highly ductile moment frames [12-13]. This work has recently been expanded upon [14-15] various bolting configurations using slotted bolted connections, focusing on the friction-slip mechanism of the bolts as the primary source for ductility and seismic energy dissipation capacity. The developed CFS MR connection, however, may be deemed incompetent with the current stud-wall LSF systems due to its manufacturing and fabrication complexities.

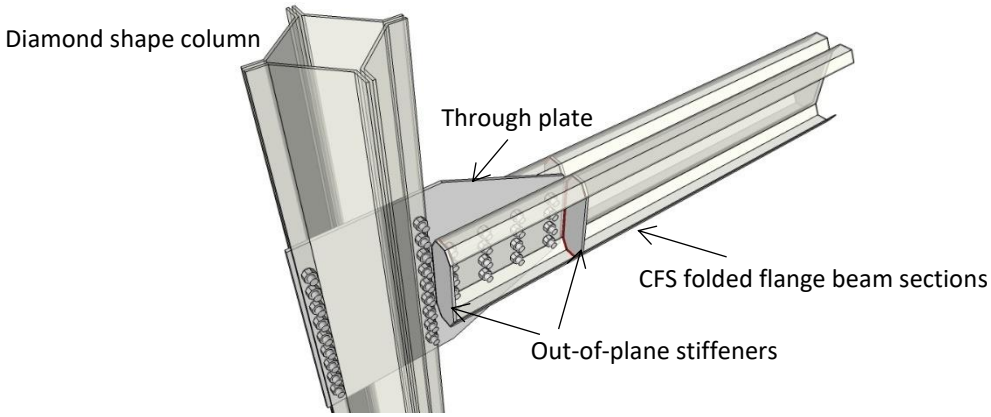

Fig. 1. Schematic view of the rigid CFS MR beam-to-column connection [7].

On the other hand, it has been revealed that [16] rubberised concrete (RuC) materials can potentially be utilised in plastic hinge zones for flexural members where high ductility is required as well as for confined compression members using steel tubes. These are mainly due to enhancement in energy dissipation capacity by increasing the rubber content and improved ductility in the post-crushing response. Within the same study [16], it was also shown that increasing the rubber content decreases the strength and stiffness, as expected. Further, a study on concrete filled steel tubes [17] shows that a higher width/thickness ratio of the steel walls can lead to a greater improvement of the column compression capacity compared with those having lower width/thickness ratios. In addition, a lower strength concrete infill can result in a more ductile behaviour compared with those infilled with higher strength concrete [17]. These studies motivate research on the development of CFS frames with relatively large width/thickness sectional elements infilled with RuC with relatively low compression strength.

In the research presented herein, the findings of the above work are integrated within the development of a new semi-rigid MR connection forming of CFS beam-to-column screwed connections with RuC filled members for a framed skeleton type of structure. With the proposed connection, local buckling of CFS beam and column sections is postponed or even eliminated due to the restraining effect of the infilled RuC, thus removing the need for complex CFS sections and out-of-plane stiffeners within the beam-to-column connections (i.e., the aforementioned connection detailing). Furthermore, compared with the bolted connections, the screwed connections can provide ease of fabrication and speed up installation which can potentially lead to a more competent LSF system.

The proposed composite CFS-RuC MR beam-to-column connection has been designed and assessed using detailed FE models subjected to both lateral and gravity loadings. A comparative parametric study has been conducted on various composite and bare steel connection configurations on their moment-rotation behaviour. The FE results have been led to a series of full-scale experimental work which has been adopted herein for FE validation purposes.

2. Detailing and design considerations for CFS-RuC beam-to-column connections

Fig. 2 shows detailing of the composite CFS-RuC semi-rigid MR connection being developed herein. The connection comprises a CFS tubular beam connected to both sides of a CFS tubular column through side plates, both having the same width. The RuC can be infilled through some filling holes that can be cut on the sides of the beam and column sections once erected onsite. The side plates can be welded offsite to the columns and screwed onsite to the beams, in a similar way to the well-known column-tree type of construction for hot-rolled steel counterparts. For a single-sided connection (like the sketch shown in Fig. 2), the side plates are extended (by around 10 mm) beyond the opposite face of the column to accommodate the flare groove weld lines which fill the rounded space between the side plate's inner surface and the channel corners. The CFS beam and column hollow rectangular sections are built up of two un-lipped channels which are connected to one another through their overlapped top and bottom flanges using self-drilling screws. These screws can be spaced at a distance less than the buckling half-wavelength of the bare steel section which can be determined through a finite strip software [18]. Fig. 3 shows the signature curves and deformed shapes of the CFS beam and column sections under bending moment and axial compression stress gradient based on 275 MPa yielding stress. The beam and column channel sections, respectively denoted by CFS300-175-2 and CFS300-175-4, both with a web height of 300 mm, an overall width of 175 mm, thicknesses of 2 and 4 mm, and each channel section with a flange width of 100 mm. An overlapped width of 25 mm has been assumed for the top and bottom flanges accommodating space for the screw fasteners attaching the two channels along their length.

The critical elastic buckling of the chosen beam and column sections correspond to the half-wavelengths of 220 mm and 260 mm having the load factors of 0.47 and 0.61, respectively. As shown in Fig. 3, the flange buckling deformations of both the beam and column sections are inward, while the webs deform outward. This indicates the possible enhancement of the local buckling resistance of the CFS sections when filled with concrete with restraining effects preventing inward buckling deformations. The obtained load factors can be inputted into Direct Strength Method

(DSM) equations, prescribed in Appendix 1 of the North American Specification AISI S100 [19], to calculate the nominal bending moment (M_n) and axial compressive strength (P_n).

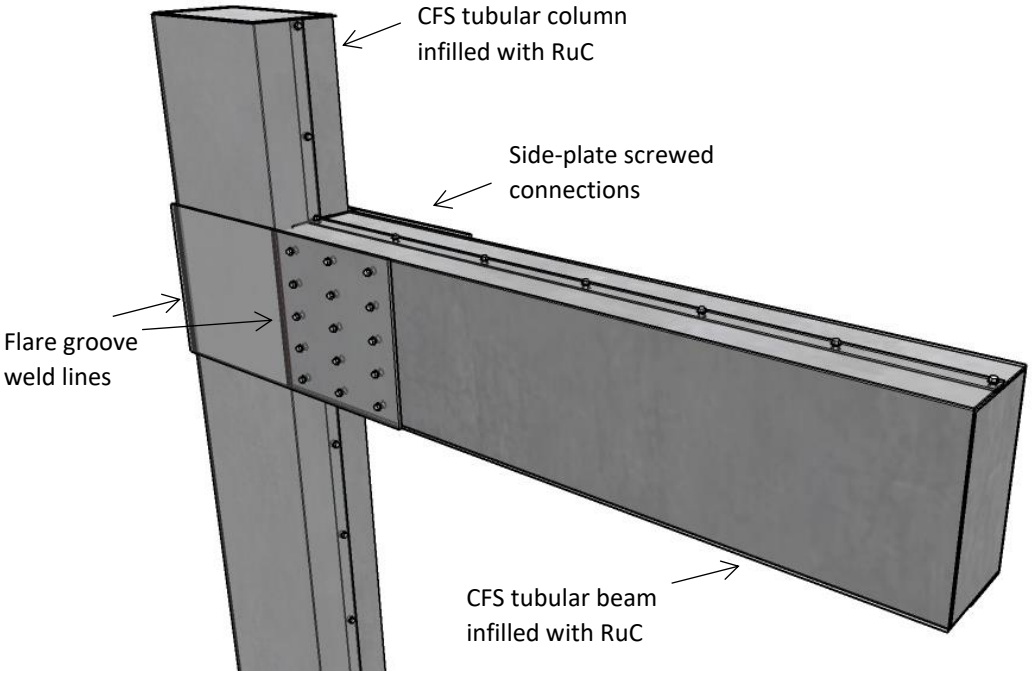

Fig. 2. Schematic view of the developed composite cold-formed steel (CFS)- rubberised concrete (RuC) moment-resisting screwed connection.

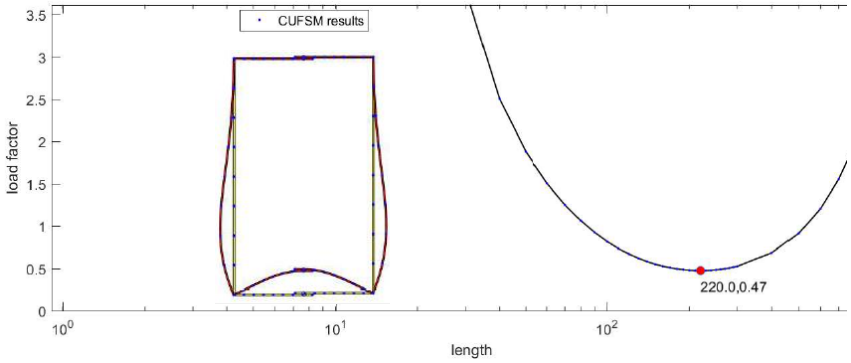

(a) CFS300-175-2 under bending moment stress gradient

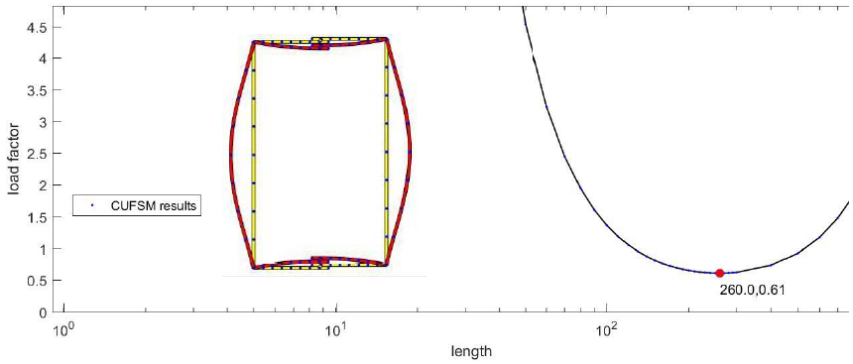

(b) CFS300-175-4 under axial compression stress gradient

Fig. 3. Elastic buckling and signature curves of the CFS (a) beam and (b) column sections.

Fig. 4 demonstrates a single-sided 2 m CFS-RuC beam representing a 4 m bay moment-resisting frame connected to a 3 m height column delineated between their inflection points subjected to lateral loading. The side plates are connected to the side faces of the column through vertical welded lines, while the beam is connected to the side plates using self-drilling #12 screw connections with 5.4 mm shaft diameter. The predicted failure limit states governing the connection design include beam local buckling (BLB), yielding and ultimate screw shear (YSS and USS) failures and side plate plasticity (SPP). The column section (CFS300-175-4) and the vertical welded lines of the side plate-to-column connection are assumed to be designed based on the well-known strong-column-weak beam concept, thus both remain elastic. Two beam sections of CFS300-175-2 and CFS300-175-3 with 2- and 3-mm thicknesses, respectively, have been considered based on which the connection components have been designed herein. The additional choice of the 3 mm beam thickness is to capture a wider range of design cases for the FE parametric study presented in the following section.

Table 1 shows various connection configurations for each of which the demand-to-capacity ratio (DCR) of the connection components have been determined. As shown in Fig. 4, the designs are based on the yielding moment of the bare steel beam ($M_{y,beam}$) assumed to be developed at the connection end projected to the connection centroid (M_{conn}) for the screw connection design and to the column face (M_{sp}) for the side plate design. This accounts for the restraining effect of the infilled RuC in prevention of the beam local buckling (shown in Fig. 3) which could possibly enable the CFS beam to reach its yielding moment. The moment strength contribution of the infilled RuC in tubular beams has been ignored due to the expected crack propagation at the tension side which would occur at both sides of the beam under cyclic loading. Various screw arrangements have been considered including two sets of 15 and 24 #12 screw arrays (for CFS300-175-2) and three sets of 24, 36 and 42 #12 screw arrays (for CFS300-175-3) at each side of the connection. The side plates have been designed using a height of 300 mm being levelled with the top and bottom flanges of the beam and a thickness range of 4, 6, and 8 mm, as described in Table 1. The steel grade of S275 has been utilised for all the steel components having the yield strength of f_y= 275 MPa, the elastic modulus of E = 203500 MPa and the Poisson`s ratio of v=0.33.

As presented in Table 1, the beam local buckling (BLB) DCRs are defined as the ratio of $M_{y,beam}$ / M_n for a bare steel beam section, where M_n is the beam nominal bending moment calculated based on DSM accounting for local/distortional buckling. This results in M_n values of 33 and 64 kN.m for the bare steel sections having 2 mm and 3 mm thicknesses, respectively. The screw connection yielding or ultimate screw shear (YSS or USS) DCRs are based on either of the ratios of $P_{s,max}$ / P_{nys} or $P_{s,max}$ / P_{nus}, where $P_{s,max}$ is the maximum screw force (see Fig. 4) resulting from M_{conn} which has been assumed to be uniformly distributed within the screw array. P_{nys} and P_{nus} are the yielding and ultimate forces of 7 kN and 10.91 kN taken from the quad-linear load-deformation backbone curve, shown in Fig. 5, which has been adopted from [20] for #12 steel-to-steel connection screw fastener. Finally, the side plate plasticity (SPP) DCRs are the ratio of M_{sp} /$M_{p,sp}$ where $M_{p,sp}$ is the side plate plastic bending moment.

As can be seen from Table 1, all the screw connection YSS DCRs are greater than those of the BLB and SPP DCRs, meaning that the screw shear mechanism is expected to be the predominant limit state for all the screw arrays for both cases of composite and bare steel connections. For the connections having 2 mm-thickness beams, BLB and/or USS could be predominant modes of failure

for the bare steel connections, while USS and/or SPP could be expected limit states for the composite connections depending on the screw arrays.

For the case of bare steel connections having 3mm-thickness beams, the SPP failure could be a predominant limit state for connections having 24, 36 and 42#12 screw arrays using SP4 and SP6, where the SPP DCR is greater than the BLB DCR. This, however, might not be the case for the connection with 24#12 having SP6 where the USS DCR of 1.78 is considerably greater than the corresponding BLB and SPP DCRs of 1.17 and 1.19, respectively. The USS DCRs for the connection with 36#12 screw array and SP6 is 1.3, which is just above the BLB and SPP DCRs, leading to a possible combination of USS-BLB-SPP failure limit state, while the same connection with SP4 has SPP DCR of 1.78 well above other DCRs which can lead to a SPP only limit state failure.

For the case of the composite connections, where the beam yielding moment is expected to be reached (i.e., the BLB DCRs are all equal to unity), the SPP limit state could govern the design for all the connections with the SPP DCRs above unity. Again, this might not be the case for the connections, where the USS DCR is noticeably greater than the SPP DCR (i.e., connections with 15#12 and 24#12 screw arrays having SP4 and SP6, respectively). These design predictions for the bare steel and composite connections are comparatively studied in the following section through detailed FE modelling.

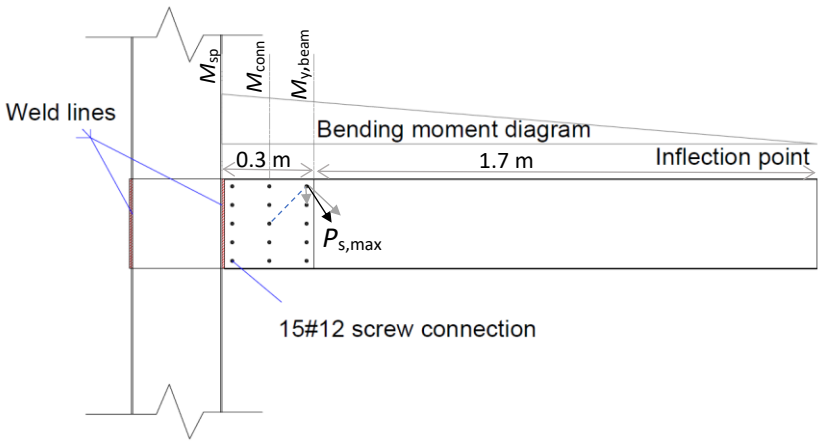

Fig. 4. Design parameters of the CFS-RuC MR connection.

Table 1. Various connection configurations and their demand-capacity ratios (DCRs; note that BLB, YSS, USS and SPP respectively stand for beam local buckling, yielding screw shear, ultimate screw shear, and side plate plasticity)

	Beam			Screw connection		Side plate (SP)	
Section	$M_{y,\ beam}$ (kN.m)	Bare steel BLB DCR	Composite DCR	Array	YSS (USS) DCRs	Thickness (mm)	SPP DCR
CFS300-175-2	50	1.52	1.0	15#12	2.61 (1.67)	4	1.19
CFS300-175-2	50	1.52	1.0	24#12	1.86 (1.19)	4	1.19
CFS300-175-2	50	1.52	1.0	24#12	1.86 (1.19)	6	0.79
CFS300-175-3	75	1.17	1.0	24#12	2.78 (1.78)	4	1.78
CFS300-175-3	75	1.17	1.0	24#12	2.78 (1.78)	6	1.19
CFS300-175-3	75	1.17	1.0	36#12	2.03 (1.30)	4	1.78
CFS300-175-3	75	1.17	1.0	36#12	2.03 (1.30)	6	1.19
CFS300-175-3	75	1.17	1.0	36#12	2.03 (1.30)	8	0.89
CFS300-175-3	75	1.17	1.0	42#12	1.78 (1.14)	6	1.19
CFS300-175-3	75	1.17	1.0	42#12	1.78 (1.14)	8	0.89

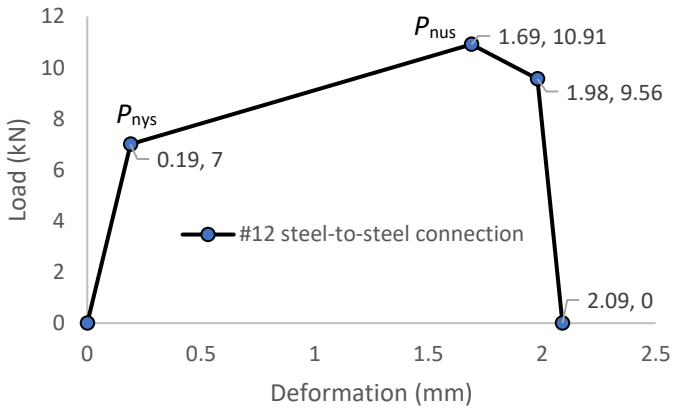

Fig. 5. Load-deformation backbone curve for #12 steel-to-steel connection [20].

3. FE studies of the bare steel and composite connections

3.1 FE modelling specifications

A detailed FE analysis using ABAQUS [21] has been employed to model the composite CFS-RuC and bare steel CFS connections designed in Section 2 having a 2 m-length cantilever beam connected to a 3 m-height column. Fig. 6 shows a typical FE model for the composite connection featuring CFS beam and column channel sections connected to one another using #12 screws as built-up tubular sections. Hinge boundary conditions with free rotation about X-direction and restrained about other rotational directions at the top and bottom end sections of the column and the free end section of the beam have been applied to the reference points RP-1-3, shown in Fig. 6. All the degrees of freedom of these end sections are coupled with the corresponding reference points. The translation in Z-direction is fixed at the top and bottom column ends RP-1 and RP-2 to resist the shear forces

and is free at the beam end RP-3. These represent the beam mid-span and the column mid-height inflection points under lateral loading condition. A constant upper storey gravity loading is applied at RP-2, while a displacement controlled lateral loading to failure of the connection is applied at RP-3, both with free translation in Y-direction. Lateral supports, representing the flooring and the orthogonal framing effects, are applied to the top flanges of the beam and the beam-column intersection surface.

The screw fasteners for beam-to-side plate screwed connections and the beam and column built-up sections are modelled using Point-based Cartesian Fasteners, available in the Abaqus library [21], with the design load-deformation backbone curve shown in Fig. 5. This modelling technique has successfully been validated by the authors in FE modelling of CFS screw connections [5]. The four vertical flare groove weld lines connecting the side plates to the column faces at both sides of the column (see Figs. 2 and 6) have been modelled using rigid Connector Beam elements. A two-step nonlinear Static General [21] analysis has been employed through which the gravity loading is applied to the column through the first step and propagated to the second step where the displacement controlled lateral loading is applied to the beam end. The linear S4R shell element was employed for all the steel sections having 4 nodes each with 6 translational and rotational degrees of freedom and reduced integration, while the RuC infill has been modelled using the 8-node reduced integration C3D8R brick element with three translational degrees of freedom per node. A mesh size of 20 mm × 20 mm was chosen for the beam and column steel channels, which has been shown [7-9] to capture the load-deformation response of CFS connections with high accuracy, while a coarser mesh size of 50 mm × 50 mm was chosen for the RuC infill. A bi-linear stress-strain curve has been utilised for all the steel components with the nominal yielding strength and modulus of elasticity same as those used at the design stage (see Section 2), and with a strain hardening second modulus ratio of E / E_s = 0.01.

A Concrete Damaged Plasticity model, available in ABAQUS [21], has been utilised to model the RuC infill which simulates both compressive crushing and tensile cracking mechanisms of the material. The mechanical properties of the RuC infill have been taken from [16] which reports on constitutive stress-strain responses of RuC materials based on monotonic and cyclic compression loading tests with total rubber content up to 40%. The compressive strength of f_{rc} = 21 MPa, the elastic modulus of E_{rc} = 14.6 Gpa and the crushing strain of $\varepsilon_{rc,0}$ = 0.16% have been adopted based on Specimen R40-S3 [16] having 40% rubber content tested under the strain rate of 1.67×10^{-2} suitable for seismic

loading. The tensile strength of 10% of the compressive strength and the Poisson`s ratio of *v*=0.2 have been assumed according to [17]. The confining pressure on the tubular sections becomes insignificant for the case of relatively large width-to-thickness ratio (greater than 15), affected by local buckling, as per [17] which is the case being studied herein.

The interaction between steel and concrete surfaces for both beam and column has been modelled using Hard contact with Penalty formulation [21]. For convergency purposes, the outer surfaces of the concrete infill with the coarser mesh defined as the master surfaces, whilst the inner surfaces of the steel walls have been defined as the slave surfaces. The element types, material models, analysis method and interaction properties adopted herein have been successfully validated against test data of concrete filled steel tubular columns with a wide range of width-to-thickness ratio between 15 and 134 [17].

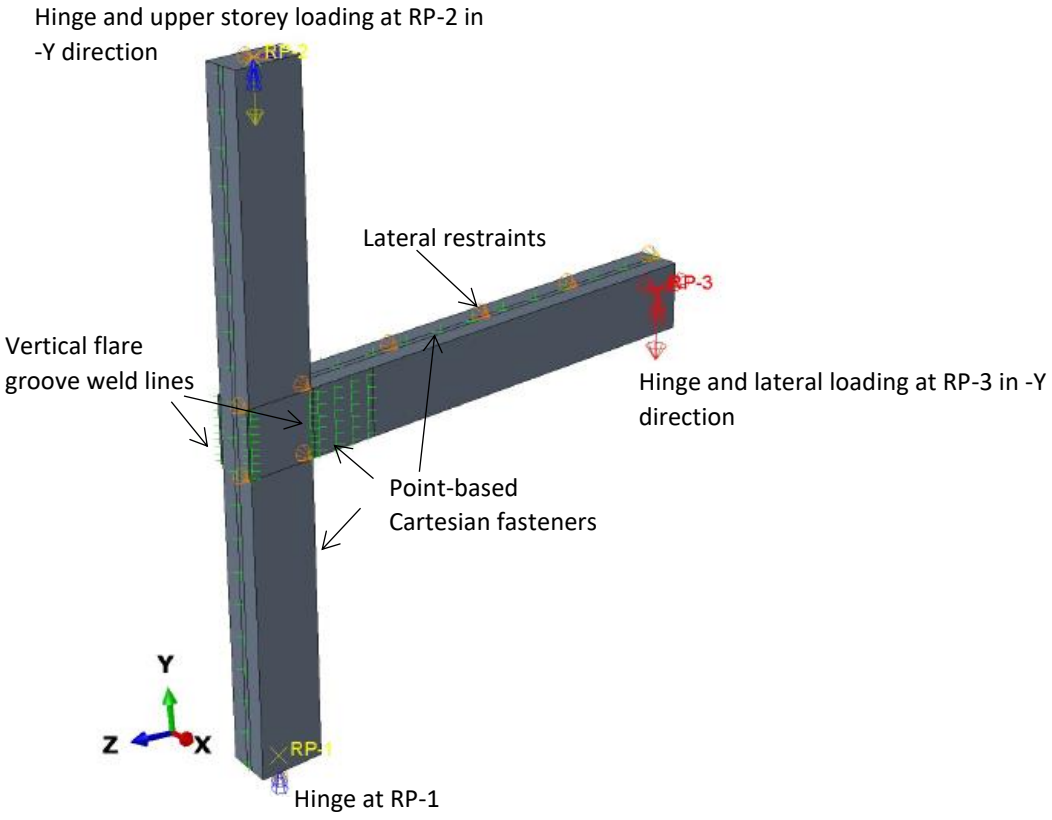

Fig. 6. Overall view for composite CFS-RuC connection FE model: Boundary conditions, loading and fasteners.

3.2 FE validation

The FE results on the developed connections presented in the following subsections have been fed into full-sized physical tests (with the overall view of the test set up shown in Fig. 7) conducted under cyclic loading at the University of Aberdeen. As can be observed, the testing specimen is a single-sided connection loaded at the free end of the testing beam with identical boundary conditions to the FE model. The testing column is supported by a strong frame at the two ends through bearing plates and rods. The focus of the experimental work, similar to the FE investigation was on the beam and screwed side-plate connection behaviour while the column was designed to remain elastic and intact as mentioned above. The testing programme included one test for each of the bare steel and composite connections which comprised CFS300-175-2 beam, and CFS300-175-4 column sections connected using SP4 side plates and 24#12 screw arrays. The choice of the testing specimens has been selected due to the different trend of responses identified for the two tested connections, as discussed later under section 3.3. The obtained moment-rotation curves and the observed modes of failures of these tests have been compared against the corresponding FE results. A more detailed results of the physical tests including the characteristics of the obtained cyclic responses and the energy dissipation of the bare steel and composite connections will be reported subsequently [22].

Fig. 8 shows the half-cycle hysteretic curves and their corresponding envelope curves for the tested composite and bare steel connections along with the relevant FE monotonic curves (shown by dashed, dotted and solid lines, respectively). It should be noted that the hysteretic curves have been offset accounting for the slackness occurred within the test set-up. Therefore, the FE monotonic curves are compared with the quadrant of the cyclic curves less affected by the set-up slackness. On comparing the results, a good agreement between the envelope of the cyclic curves of the tested specimen and the FE monotonic curves can be identified on their overall trend, initial stiffness, and the peak moment. The differences could be due to the deviations between the CFS and RuC material properties, load-deformation behaviour of the screws in the tests and those assumed in the FE taken from [20], and the cyclic loading effects. These have led to around 5% and 10% higher peak moment strengths for the FE composite and bare steel connections, respectively, compared with their corresponding tested connections. A sharper strength degradation and, as a result, a lower ductility capacity can also be identified in the test hysteretic curves compared with the FE monotonic curves which could be due to the cyclic loading effects. It should be noted that the FE studies presented herein have been conducted prior to the tests on the concept development of the CFS-RuC connections. However, an updated FE study is required to further investigate the identified sources of discrepancies between the test and FE results.

The predominant modes of failures for the composite and bare steel connections were yielding and ultimate screw shear (YSS-USS) (Fig. 9 (a)) and the beam local buckling (BLB) (Fig. 9 (b)) which agree with those predicted through the corresponding FE analysis. The YSS-USS failure can be identified by comparing the relative rotation between the beam and the side plate through the white line (shown in Fig. 9 (a)) which was initially aligned with the vertical edge of the side plate.

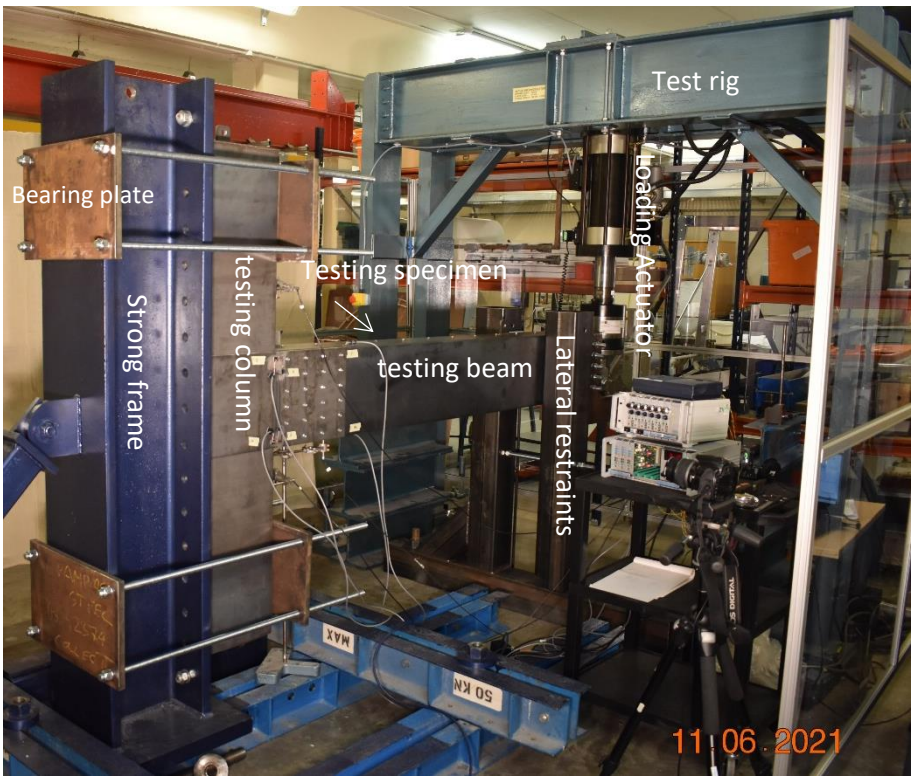

Fig. 7. An overall view of the developed connection test set up at the University of Aberdeen.

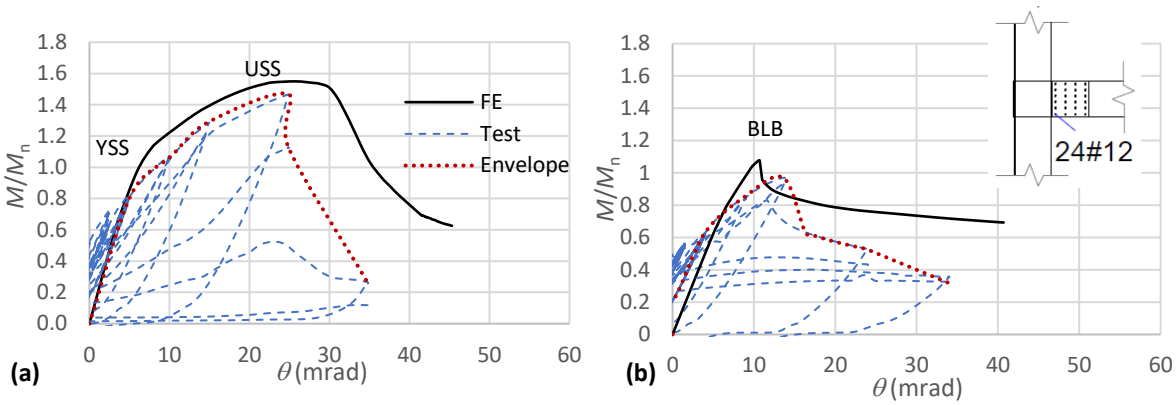

Fig. 8. Comparison between test and FE moment-rotation behaviour for (a) composite and (b) bare steel connections having CFS300-175-2 and CFS300-175-4 beam and column sections, SP4 side plates and 24#12 screw arrays.

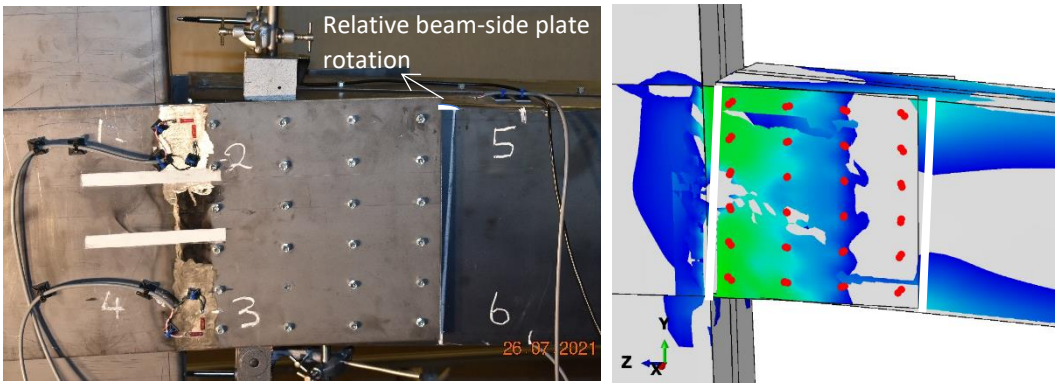

(a) YSS-USS in composite connections

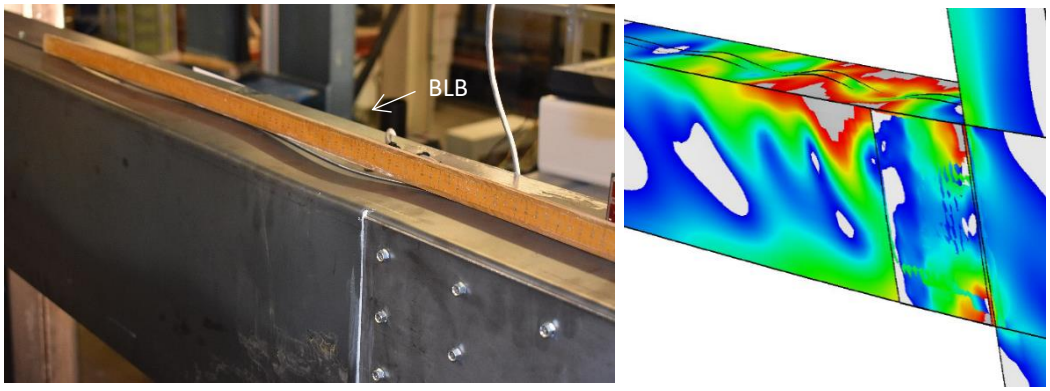

(b) BLB in bare steel connections

Fig. 9. Test and FE failures of the (a) composite and (b) bare steel connections having CFS300-175-2 and CFS300-175-4 beam and column sections, SP4 side plates and 24#12 screw arrays.

.

3.3 FE results and discussions

FE analysis was conducted for the designed connections in Section 2 using CFS300-175-2 or 3 beams connected to a CFS300-175-4 column through 4 mm, 6 mm or 8 mm thickness side plates using a range of 15, 24, 36 and 42 #12 screw arrays presented in Table 2. Both bare CFS and composite CFSRuC connections were modelled for comparison purposes investigating the effect of the infilled RuC on the connection load-deformation response. The FE models (listed in Table 2) are labelled with the start abbreviations of CFS or CFSRuC and the beam and column thicknesses (2-4 or 3-4 mm), respectively, followed by side plate thicknesses (SP4, 6 or 8 mm) ended by the number of the screw connection arrays (#15, 24, 36 or 42). A displacement controlled monotonic loading was applied to the beam end until connection failure representing the frame lateral loading. Three levels of 60, 300 and 600 kN gravity loading were applied to the column representing the flooring dead and live loads of 5 and 2.5 kN/m^2, respectively, corresponding to 1, 5 or 10 floors above the column with a tributary area of 4 × 2 m for each floor. It is assumed that the gravity loads are transferred to the column through the orthogonal beams of the single-sided connection model. The share of the infill RuC in the calculated gravity loads of the considered floor area was around 2.2 kN for each floor level. This indicates the infill RuC may not have a noticeable impact on the overall weight of such structures.

Table 2. CFS and CFS-RuC connection models

Label	Steel beam section	Side plate dimensions	Screw connection	
CFS2-4-SP4#15	CFS300-175-2	620 × 300 × 4	15#12	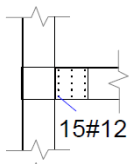
CFSRuC2-4-SP4#15	CFS300-175-2	620 × 300 × 4	15#12	
CFS2-4-SP4#24	CFS300-175-2	620 × 300 × 4	24#12	
CFSRuC2-4-SP4#24	CFS300-175-2	620 × 300 × 4	24#12	
CFS2-4-SP6#24	CFS300-175-2	620 × 300 × 6	24#12	
CFSRuC2-4-SP6#24	CFS300-175-2	620 × 300 × 6	24#12	
CFS3-4-SP4#24	CFS300-175-3	620 × 300 × 4	24#12	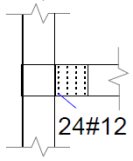
CFSRuC3-SP4-4#24	CFS300-175-3	620 × 300 × 4	24#12	
CFS3-4-SP6#24	CFS300-175-3	620 × 300 × 6	24#12	
CFSRuC3-4-SP6#24	CFS300-175-3	620 × 300 × 6	24#12	
CFS3-4-SP4#36	CFS300-175-3	620 × 300 × 4	36#12	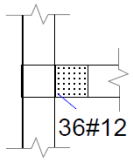
CFSRuC3-4-SP4#36	CFS300-175-3	620 × 300 × 4	36#12	
CFS3-4-SP6#36	CFS300-175-3	620 × 300 × 6	36#12	
CFSRuC3-4-SP6#36	CFS300-175-3	620 × 300 × 6	36#12	
CFS3-4-SP8#36	CFS300-175-3	620 × 300 × 8	36#12	
CFSRuC3-4-SP8#36	CFS300-175-3	620 × 300 × 8	36#12	
CFS3-4-SP6#42	CFS300-175-3	620 × 300 × 6	42#12	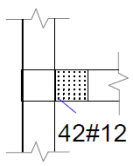
CFSRuC3-4-SP6#42	CFS300-175-3	620 × 300 × 6	42#12	
CFS3-4-SP8#42	CFS300-175-3	620 × 300 × 8	42#12	
CFSRuC3-4-SP8#42	CFS300-175-3	620 × 300 × 8	42#12	

3.3.1 FE results for connections with 2 mm beam thickness

Fig. 10 shows the normalised bending moment (M / M_n) - rotation (θ) responses along with the corresponding normalised screw forces (P_s / P_{nys}) for the CFS and CFSRuC connections having 2 mm beam thickness (with M_n = 33 kN.m and P_{nys} = 7 kN), 4 mm side plate thickness (SP4) and 15#12 screw array. M is the beam bending moment calculated at the connection end, while θ is the sum of beam and connection rotation determined at the connection centroid (see Fig. 4) subtracted by the column rotation. As it can be observed, both the bare steel and composite connections (shown by dashed and solid lines, respectively) have slightly exceeded their nominal bending moment capacity (based on DSM) and reached M_{peak} / M_n = 1.04 and 1.01, at around θ_{peak} = 19 and 14 mrad rotation, respectively, after which both connections degrade with a similar trend. The reason being, both connections are governed by the USS limit state (reflected by the highest DCR in Table 1) leading to complete screw failure (i.e., corresponding to the last point with a deformation value of 2.09 mm in Fig. 5).

As an indication of the ductility capacity defined by a factor of $\mu = \theta_u / \theta_y$, it is assumed herein that the connection yielding (θ_y) occurs at the rotation where the screws reach their yielding capacity and that the ultimate rotation (θ_u) is where the connection post-peak strength reaches 80% of M_{peak}. Based on these, the ductility capacity of μ = 4.6 and 3.96 have been achieved for the bare steel and composite connections using 15#12 screw array, respectively. The presented values in Table 3 are the results for M_{peak} / M_n, θ_{peak}, θ_y, θ_u and μ as well as the failure limit states for all the bare steel and composite connections listed in Table 2.

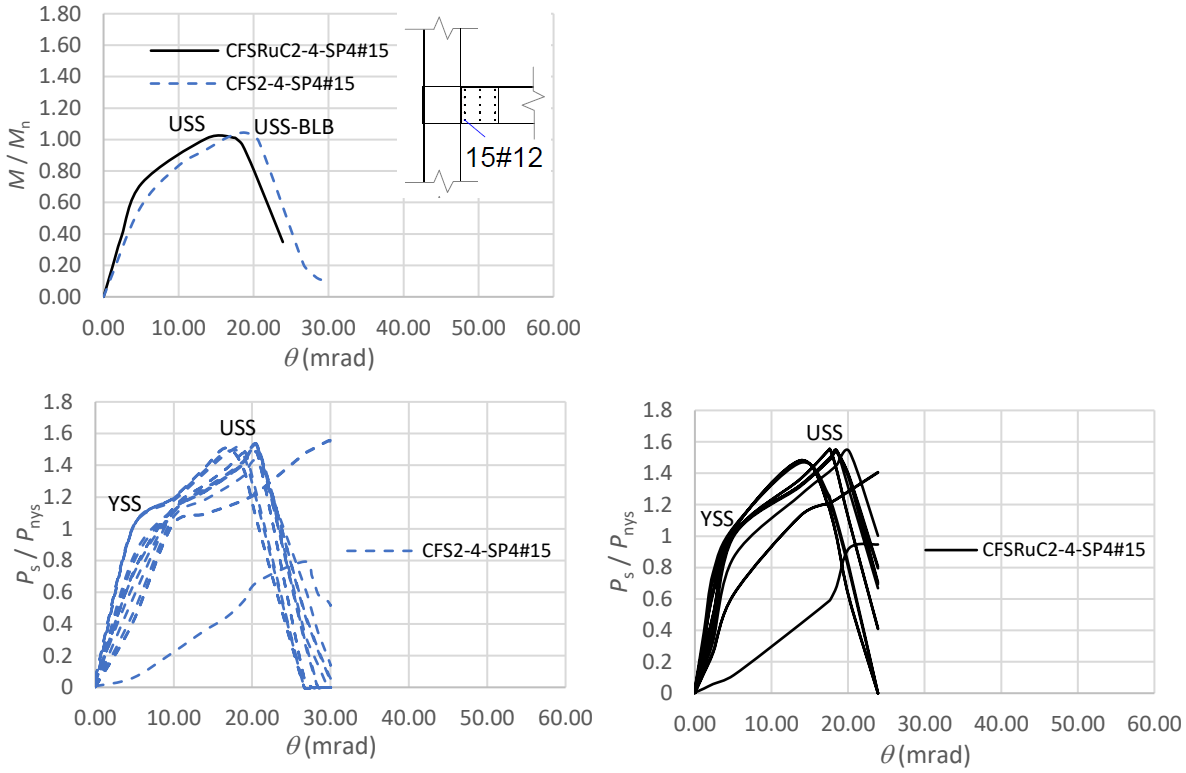

Fig. 10. Normalised M / M_n - θ and P_s / P_{nys} - θ curves for CFS and CFSRuC connections having 2 mm beam thickness, SP4 and 15#12 screw array.

Table 3. Results for bare steel and composite connections

Label	M_{peak} / M_n	θ_{peak} (mrda)	θ_y (mrda)	θ_u (mrda)	$\mu = \theta_u / \theta_y$	Failure
CFS2-4-SP4#15	1.04	19	4.77	22	4.6	USS-BLB
CFSRuC2-4-SP4#15	1.01	14	5.09	20.17	3.96	USS
CFS2-4-SP4#24	1.08	10	5.93	14	2.36	BLB
CFSRuC2-4-SP4#24	1.55	26	3.7	32	8.65	USS-SPP
CFSRuC2-4-SP6#24	1.58	17	5.91	22	3.72	USS
CFS3-4-SP4#24	0.74	18	4.61	33	7.18	USS-SPP
CFSRuC3-SP4-4#24	0.79	24	5	29	5.8	USS-SPP
CFS3-4-SP6#24	0.79	20	4.05	22	5.43	USS
CFSRuC3-4-SP6#24	0.83	17	4.62	21	4.55	USS
CFS3-4-SP4#36	0.76	15	5.18	36	6.95	SPP
CFSRuC3-4-SP4#36	0.79	16	5.54	62	11.19	SPP
CFS3-4-SP6#36	1.11	23	4.92	27	5.49	USS-SPP-BLB
CFSRuC3-4-SP6#36	1.14	21	4.55	27	5.93	USS-SPP
CFS3-4-SP8#36	1.11	19	6	23	3.83	USS-BLB
CFSRuC3-4-SP8#36	1.08	15	4.53	24	5.29	USS
CFS3-4-SP6#42	1.12	20	6.5	22	3.38	SPP-BLB
CFSRuC3-4-SP6#42	1.24	29	4.53	53	11.70	USS-SPP
CFS3-4-SP8#42	1.22	19	6.5	28	4.30	BLB
CFSRuC3-4-SP8#42	1.25	17	4.5	26	5.78	USS

Fig. 11 shows the von-Mises stress contours at M_{peak} for both the bare steel and composite connections of CFS2-4-SP4#15 and CFSRuC2-4-SP4#15 under the constant column gravity loads of 60, 300 and 600 kN. The areas with stress level greater than the yielding limit (i.e., 275 MPa) are shown by grey colour. It can be observed that local buckling occurs within the bare steel beams at around M_{peak} / M_n =1, matching the DSM design prediction, whilst the RuC infill effectively prevents the beam local buckling. The projected peak bending moment in the beam to the connection centroid triggers the USS force of 10.91 kN (see Fig. 5). This leads to the screw shear degradation starting at P_s / P_{nys} = 1.56 (see screw forces in Fig. 10) which corresponds to P_s / P_{nus} = 1.0 resulting in the similar moment-rotation responses for both bare steel and composite connections. It can also be seen that, at around M_{peak} / M_n, yielding stress has been developed within the top and bottom areas of the side plates (reflecting the lowest side plate plasticity (SPP) DCR in Table 1).

Fig. 11 also shows the von-Mises contours for the bare steel and composite columns. As can be observed, the stress level increases by increasing the gravity loads leading to a column buckling within the bare steel column under the gravity load of 600 kN. This could be predicted through a simplified interaction equation of P_c / ($P_{n,\,CFS}$ + $P_{n,\,RuC}$) + M_c / $M_{n,CFS}$, where P_c and M_c are respectively the column axial force and the projected bending moment to the column centroid; $P_{n,CFS}$ and $M_{n,CFS}$ are the DSM nominal compression and bending moment strengths of the CFS section; and, $P_{n,\,RuC}$ is the compression strength of RuC infill, whilst its moment strength contribution has been conservatively ignored which is in consistent with the assumption for the composite beams as indicated in Section 2.

For the case of bare steel CFS300-175-4 column section $P_{n,CFS}$ and $M_{n,CFS}$ are respectively equal to 740 kN and 98 kN.m calculated through DSM equations [19]. For the case of composite CFSRuC300-175-4, these are assumed as the CFS yielding strength of 1100 kN for the axial compression, while $M_{n,CFS}$ equals to $M_{y,column}$. $P_{n,\,RuC}$ can be calculated as $f_{rc} \times A_c$ = 1103 kN, where f_{rc} is the RuC material's compression strength assumed as 21 MPa and A_c is the section area. Based on these, the bare steel column DCRs are 0.56, 0.88, and 1.28, when subjected to axial gravity loads of 60, 300 and 600 kN, respectively, while the composite column DCRs are 0.47, 0.58 and 0.74. As can be seen, the bare steel column DCR under the gravity load of 600 kN exceeds unity indicating the occurrence of the column local buckling. This highlights the efficiency of the RuC infill for the CFS columns, which can eliminate local buckling and significantly reduce the DCR by up to 42%. If the contribution of the infilled RuC in compression strength was ignored (i.e., $P_{n,\,RuC}$ = 0), the composite column DCRs, based on the modified interaction equation of P_c / $P_{n,\,CFS}$ + M_c / $M_{n,CFS}$, would be then increased to 0.51, 0.72, and 1.02. These values still show a considerable reduction compared to those of the bare steel columns by up to 20% due to the increase in $P_{n,CFS}$ compression strength up to its yielding level.

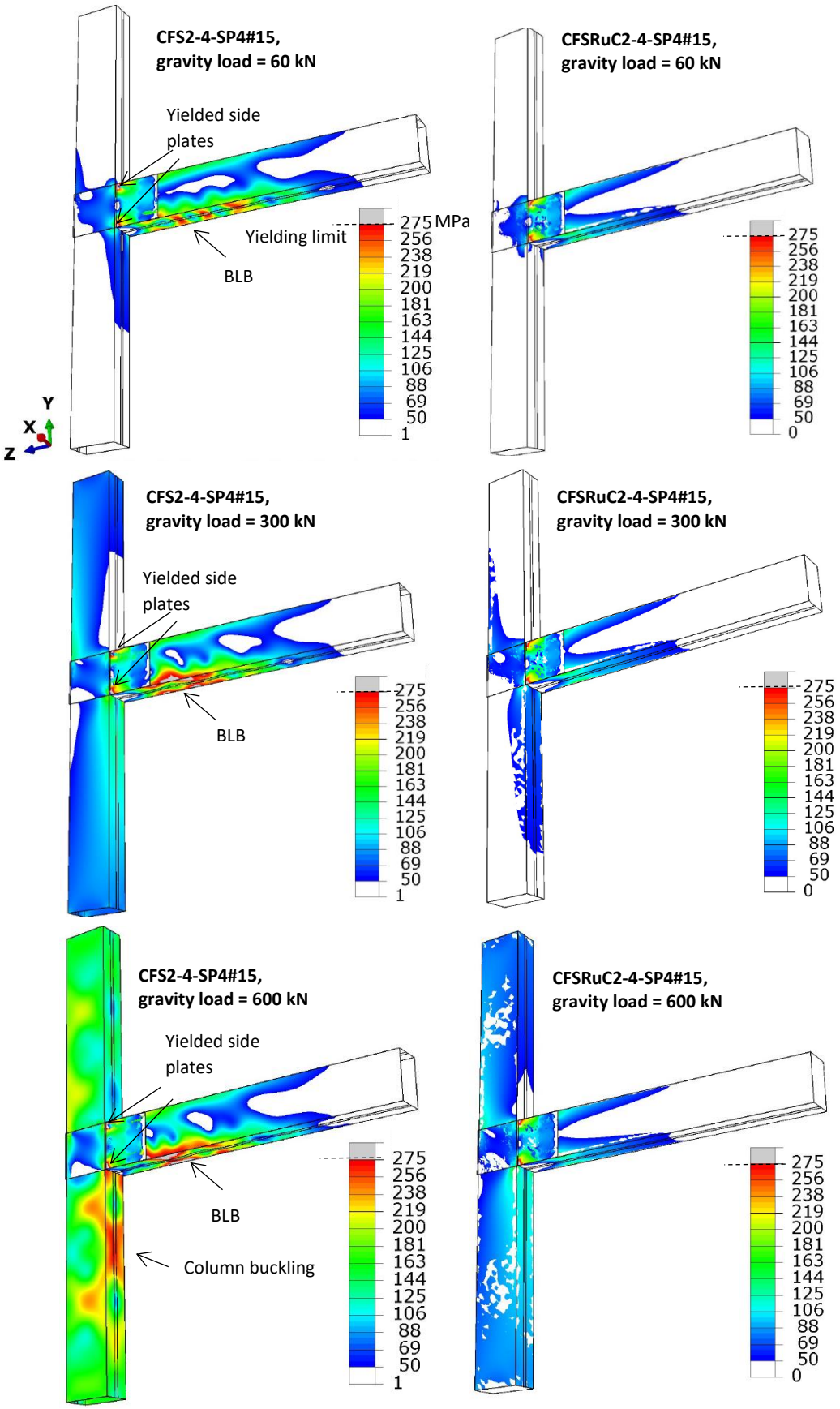

Fig. 11. Von-Mises stress contours (displayed in MPa) at M_{peak} for CFS2-4-SP4#15 and CFSRuC2-4-SP4#15 connections under column gravity loads of 60, 300 kN and 600 kN.

By increasing the number of screws from 15#12 to 24#12, BLB DCR (i.e., 1.52) would become greater than the ultimate screw shear (USS) DCR (i.e., 1.19; see Table 1), and thus has solely governed the moment-rotation response of the bare steel connection (i.e., CFS2-4-SP4#24), as can be seen in Figs. 12 and 13. The M_{peak} / M_n reaches 1.08 at around θ_{peak} = 10 mrad followed by a sharp strength degradation due to the local buckling, resulting in a relatively low ductility factor of μ = 2.36. Although the screw shear forces exceed the yielding limit (i.e., P_s / P_{nys} = 1.0) at an earlier rotation around θ_y = 5.93 mrad, they have not reached their ultimate force of 10.91 kN (corresponding to P_s / P_{nys} = 1.56) due to the governing BLB limit state in the bare steel.

The composite CFSRuC2-4-SP4#24 connection, on the other hand, shows a significant improvement in both the moment-rotation response (see Fig. 12) reaching M_{peak} / M_n = 1.55 at around the rotation of θ_{peak} = 26 mrad and the ductility factor reaching μ = 8.65 which are respectively 44% and 2.67 times greater than those of the bare steel connection counterpart. The side plate plasticity (see CFSRuC2-4-SP4#24 in Fig. 13), deemed herein as the desirable limit state, governs the moment-rotation response of the composite connection, also indicated by the side plate plasticity (SPP) DCR of 1.19 in Table 1. The screw shear forces for CFSRuC2-4-SP4#24 exceeded their YSS limit at an earlier rotation of θ_y = 3.7 mrad; reached their USS and sustained their strength enabling an extensive degree of plasticity to be developed within the side plates.

By increasing the side plate thickness in the composite connection from 4 to 6 mm (shown by thicker solid line curves in Fig. 12), M_{peak} / M_n slightly increases to 1.58 at an earlier rotation of θ_{peak} = 17 mrad due to the increased stiffness of the connection. The governing limit state, however, has been shifted from USS-SPP to USS only (see CFSRuC2-4-SP6-24#12 in Fig. 12) reaching θ_u at around 22 mrad which leads to a reduced ductility factor of μ = 3.72 compared with that of the CFSRuC2-4-SP4-24#12 composite connection. The side plates remain intact with limited yielding at the top and bottom areas (shown in Fig. 13) which is not deemed as a desirable design.

Therefore, as a recommendation in the design of the developed composite connections, the side plates should reach their plastic capacity (SPP) prior to the screws reaching their ultimate shear force capacity (USS). The concurrent USS-SPP limit state (similar to the design for CFSRuC2-4-SP4-24#12) might not be practically achievable due to the possible connection imperfections and design uncertainties, thus the aforementioned recommendation prioritising occurrence of SPP over USS.

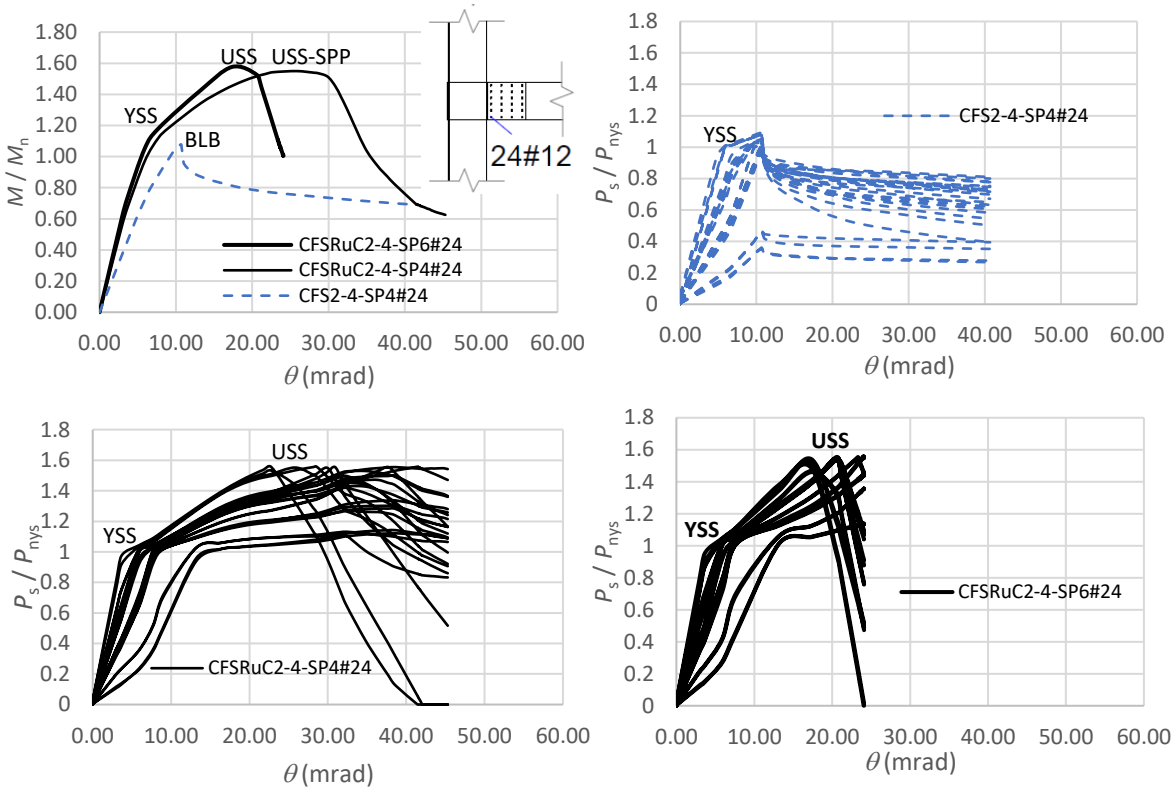

Fig. 12. Normalised M / M_n - θ and P_s / P_{nys} - θ curves for CFS and CFSRuC connections having 2 mm-beam thickness, SP4, SP6 and 24#12 screw array.

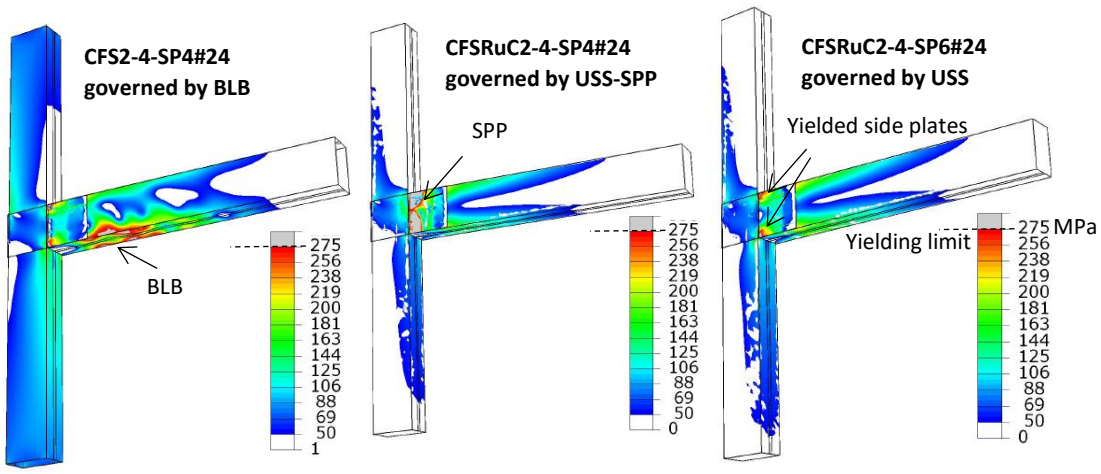

Fig. 13. Von-Mises stress contours (displayed in MPa) at M_{peak} for CFS2-4-SP4#24, CFSRuC2-4-SP4#24 and CFSRuC2-4-SP6#24 connections under the column gravity load of 300 kN.

3.3.2 FE results for connections with 3 mm beam thickness

Fig. 14 shows the normalised moment – rotation responses for the bare steel and composite connections of the 3 mm thickness beam (with M_n = 64 kN.m) connected to the 4 mm thickness column using either of 4 mm, 6 mm, and 8 mm side plate thicknesses and 24, 36 and 42#12 screw arrays (listed in Table 2). All the connections using 24#12 screw array have been governed by ultimate screw shear (USS) limit state, also predicted in the design by the USS DCR = 1.78 which is considerably higher than the bare steel beam local buckling (BLB) DCR of 1.17 (see Table 1). Therefore, no local buckling occurred in the beams with the M_{peak} / M_n lower than unity in the range of 0.74-0.83. The USS limit state has been concurrent with the desirable side plate plasticity (SPP) limit state for both the bare steel and composite connections with 4 mm side plate thickness (i.e., CFS3-4-SP4#24 and CFSRuC3-4-SP4#24). The screw shear forces, as shown in Fig. 14 for the example of CFS3-4-SP4#24, reached YSS-USS and sustained strength enabling relatively large ductility factors of μ = 7.18 and 5.8 (see Table 3) for the bare steel and composite connections, respectively. By increasing the SP thickness from 4 to 6 mm (shown by thicker lines in Fig. 14), however, the SPP DCR (see Table 1) has been reduced to 1.19 leading to the USS only limit state to govern the moment-rotation response through a relatively sharp strength degradation for both CFS3-4-SP6#24 and CFSRuC3-4-SP6#24 connections. These results show that for the designs where the BLB limit state does not govern the use of RuC infill might not be effective.

By increasing the number of screws from 24#12 to 36#12 and using SP4, SPP governs the moment-rotation response (as predicted in Table 1) which limits the M_{peak} / M_n to 0.76 and 0.79 for the bare steel and composite connections, respectively. The SPP limit state, however, provides a high ductility factor of μ = 6.94 and 11.19 with a relatively smooth degradation after the peak moments (see Fig. 14). By using 36#12 screws and SP6, USS marginally governs the connection response (see Fig. 14 for the CFS3-4-SP6#36 screw force example graph) with the DCR of 1.3, which is just above the bare steel BLB DCR of 1.17 and SPP DCR of 1.19 (see Table 1). As a result, both the SPP-BLB and SPP limit states concurrently developed with the USS limit state for the bare steel and composite connections, respectively (see Fig. 14). For the connection with 36#12 screws and SP8 (shown by the thickest solid and dashed lines in Fig. 14), however, a limited yielding occurred at the top and bottom areas of the side plates. Therefore, the bare streel and composite connection responses have been governed by the USS-BLB and USS only, respectively. The M_{peak} / M_n slightly exceeded unity within the range of 1.08-1.14, also consistent with the DSM predictions with a reasonable safety margin. The ductility factors, as expected, were greater for the SP4 connections compared with the ones for SP6 and SP8

connections by up to 1.81 and 2.11 times for the bare steel and composite connections, respectively (see Table 3).

Finally, the screw forces of the bare steel connections using 42#12 and SP6 (see CFS3-4-SP6#42 in Fig. 14) reached P_s / P_{nys} = 1.34 which is less than the ratio of 1.56 corresponding to the USS force of 10.91 kN. This has also been reflected within the design showing slightly lower USS DCR of 1.14 compared with the BLB DCR of 1.17 (see Table 1). The BLB limit state, therefore, governs the moment-rotation response of the bare steel connections, while the composite connections have been governed by USS with the eliminated beam local buckling. These have been combined with SPP for the lower thickness SP6 connections, whereas the side plates with 8 mm thickness remain largely intact with limited yielded areas. The M_{peak} / M_n for all the connections exceeded unity within the range of 1.12-1.25 with the composite connections reached their yielding moment capacity. The composite connection with the lower SP thickness of 6 mm resulted in the ductility factor of μ = 11.7 which is 3.46 times greater than that of its bare steel connection counterpart. This again indicates the effectiveness of the RuC infill particularly for the bare steel connections governed by BLB limit state, where the composite connection eliminates the beam local buckling and significantly improves the connection response leading to a desirable USS-SPP limit state.

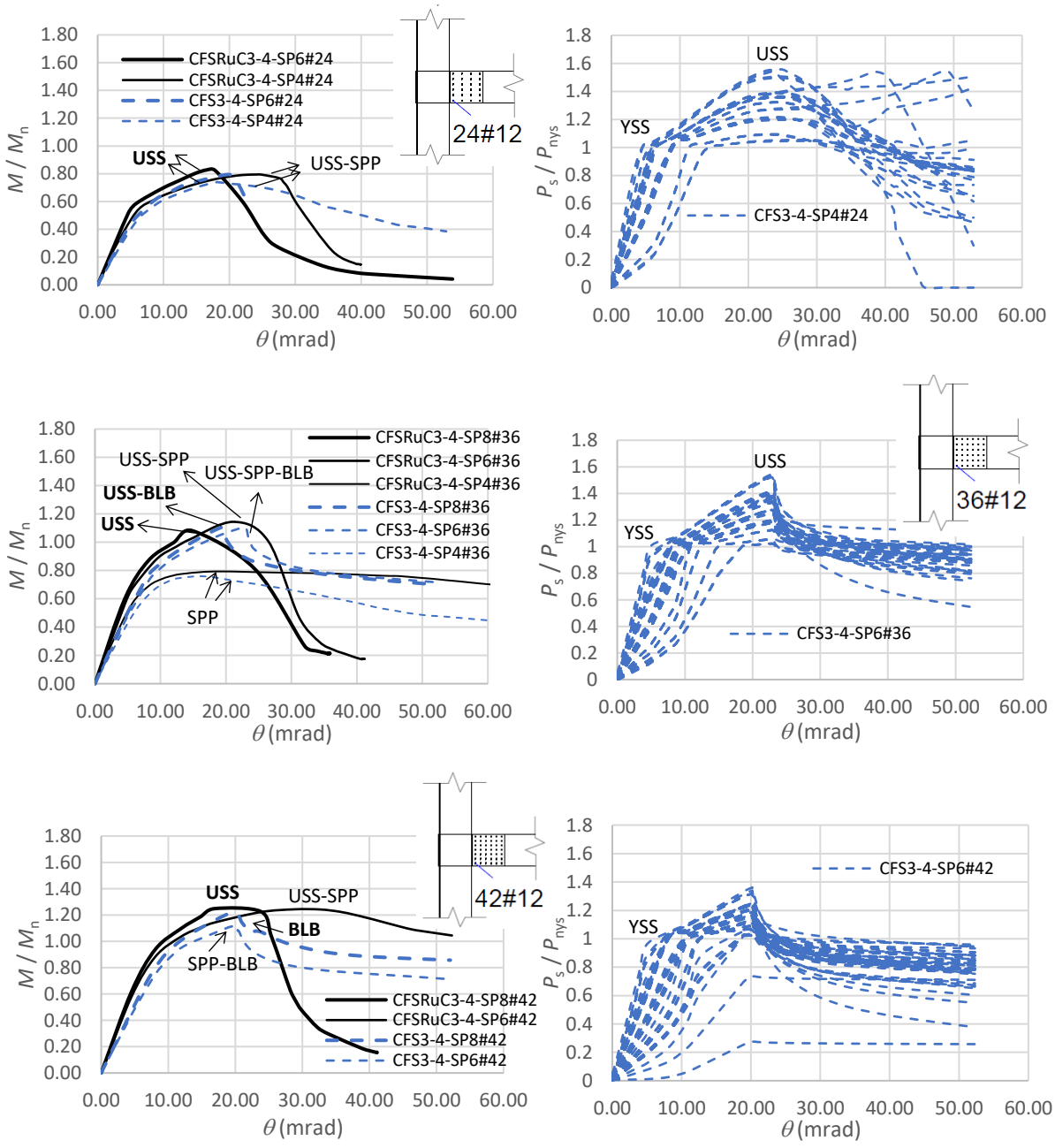

Fig. 14. Normalised M / M_n - θ and example P_s / P_{nys} - θ curves for CFS and CFSRuC connections having 3 mm beam thickness, SP4, SP6, SP8 (differentiated by increasing the thickness of the curves), and 24, 36 and 42#12 screw arrays.

3.3.3 FE results for weld line forces

To avoid a brittle side plate-to-column welding failure limit state, a reasonable assumption on the load transferring mechanism between the side plate and the column is required to be known for a reliable design of the weld lines. Fig. 15 shows the weld line coupling forces of the near and opposite column faces (at each side of the connection, shown by dashed lines) derived from the FE models for the representative bare steel and composite connections of CFS3-4-SP6#42 and CFSRuC3-4-SP6#42. Also shown in Fig. 15 (by solid lines) are the weld line forces based on the assumption of fully in-plane load transferring mechanism calculated from the projected bending moment at the centre of the column (see Fig. 4) divided by the column depth. Based on these, the bending moment resulting from the weld line coupling forces from FE constitutes around 45%, on average, of the total bending moment transferred to the column. The remaining 55% share of the bending moment would be transferred through the out-of-plane mechanism to the near face weld lines, which needs to be accounted for when designing the welded connection. The connection shear force is also fully resisted by the near face weld lines. It should be noted that the FE near face coupling forces, shown in Fig. 15, have been subtracted by the beam shear.

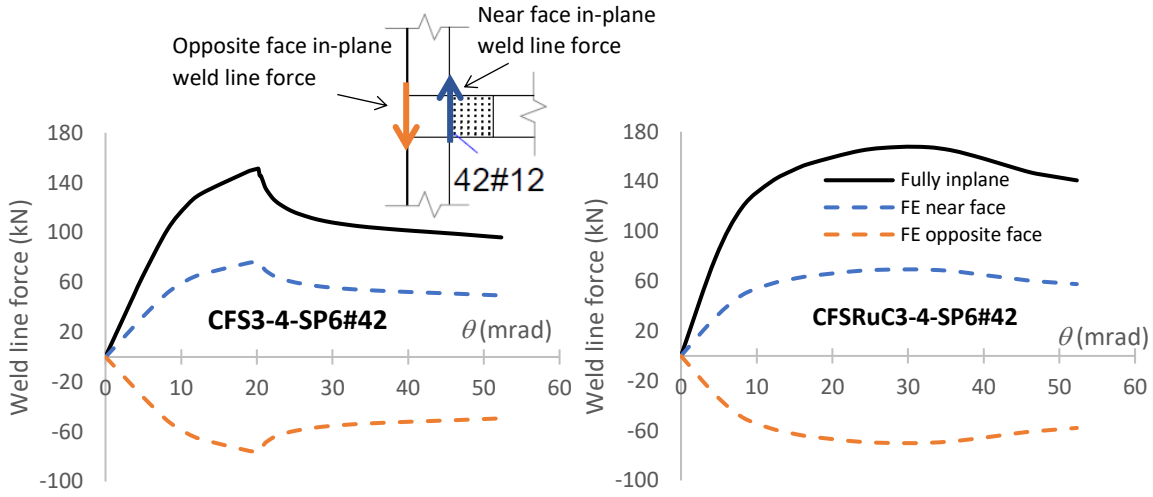

Fig. 15. Weld line forces for the CFS3-4-SP6#42 and CFSRuC3-4-SP6#42 connections.

3.3.4 Joint classification

To assess the connection rigidity the initial elastic stiffness of the connections has been compared against the limits specified in Eurocode 3-part 1-8 [23] for simple and rigid joints. These are $S_{j,ini}$= 0.5 EI_b / L_b and $S_{j,ini}$= 25 EI_b / L_b, where EI_b and L_b are the bending rigidity and the length of the beam, respectively. A semi-rigid joint is defined when the connection elastic stiffness lies within the specified limits. Fig. 16 shows the relative beam-column connection rotation of both the bare steel

and composite connections, determined over the elastic region, versus the bending moment of M_c, calculated at the connection centroid. As can be observed all the moment-rotation curves for bare steel and composite connection with various screw arrays are located within the semi-rigid joint region. In general, the composite connections (shown by solid lines) produced greater stiffness than their corresponding bare steel connections (shown by dashed lines). Further by increasing the number of connection screws the connection stiffness has been increased.

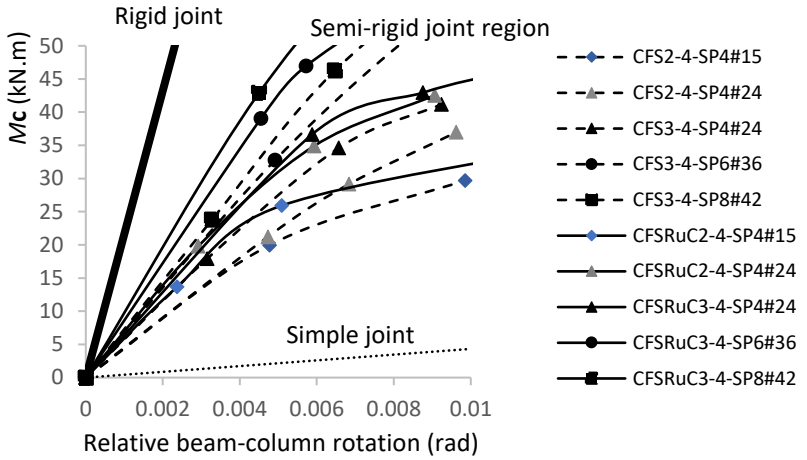

Fig.16. Rigidity of the composite and bare steel connections.

4. Conclusions

By means of finite element (FE) analysis validated against physical tests, a composite cold-formed steel (CFS)-rubberise concrete (RuC) moment-resisting beam-to-column connection has been developed. The connection comprises tubular built-up CFS channels infilled with RuC connected using side plates welded to both faces of column and screwed to the beam webs. Displacement controlled lateral loading has been applied to the beam end until the connection failure, whilst the column has been loaded under gravity loading. The beam channels had 2 mm and 3 mm thicknesses connected to a 4 mm thickness column, both with the overall section depth and width of 300 and 175 mm, respectively. A range of 4 mm, 6 mm and 8 mm side plate thicknesses and screw arrays of 15, 24, 36 and 42#12 have been comparatively assessed for both bare steel and composite connections. The identified failure limit states included beam local buckling (BLB), yielding and ultimate screw shear (YSS and USS) and side plate plasticity (SPP).

It was shown that the infilled RuC can effectively eliminate the BLB limit state leading to an improved moment-rotation response. The moment strength and ductility capacity of the composite connections governed by USS-SPP limit states were up to 1.44 and 3.46 times greater than those of the bare steel connections governed by BLB limit state, respectively. It was also shown that the column strength can be increased by up to 42% when infilled compared with the bare steel columns due to the elimination of local buckling and RuC contribution towards the axial compression strength of the column. Further, using lower thickness SP, governed by SPP, can lead to higher ductility capacity compared with those of the larger thickness SP connections, typically governed by USS-BLB and USS, by up to 1.81 and 2.11 times for the bare steel and composite connections, respectively.

It was revealed that the side plate-to-column welded connection can be designed based on 45% of the bending moment at the column centre transferred through in-plane coupling forces resisted by the near and opposite face weld lines, while a 55% share remains for the out-of-plane force distribution resisted by the near face weld lines. The beam shear force is fully resisted by the near face weld lines.

The connection rigidity has been assessed and showed that both the bare steel and composite connections can be classified as a semi-rigid joint. Further, the composite connections typically produced a higher connection stiffness compared with the corresponding bare steel connections.

Acknowledgement

This research was supported by the Royal Academy of Engineering Frontiers of Development Seed Funding scheme (FoD2021\4\26). The connection drawing by MSc student Dieudonne Iraghua at Ozyegin University was much appreciated.

Disclaimer

Any opinions, findings, and conclusions or recommendations expressed in this publication are those of the authors and do not necessarily reflect the views of the sponsors and employers.

References

[1] SCI Publication P402, Light steel framing in residential construction, ISBN 13: 978-1-85942-215-1, 2015.

[2] Hough MJ., Lawson RM. (2019). Proceedings of the Institution of Civil Engineers - Civil Engineering, 172(6), 17–44.

[3] R.L. Madsen, N. Nakata, B.W. Schafer (2011). CFS-NEES Building Structural Design Narrative, Research Report, RR01, access at www.ce.jhu.edu/cfsnees.

[4] D. Ayhan, BW. Schafer (2019). Cold-formed steel ledger-framed construction floor-to-wall connection behaviour and strength. Journal of Constructional Steel Research. 156, 215-226.

[5] A. Bagheri Sabbagh, S. Torabian (2021). "Semi-rigid floor-to-wall connections using side-framed lightweight steel structures: Concept development", Thin-Walled Structures, 160,107345.

[6] Uang C-M, Sato A., Hong J-K, Wood K. (2010). Cyclic testing and modeling of cold-formed steel special bolted moment frame connections, Journal of Structural Engineering, Vol. 136, No. 8, 953-960

[7] A. Bagheri Sabbagh (2011). Cold-formed steel elements for earthquake resistant moment frame buildings, PhD thesis, University of Sheffield

[8] A. Bagheri Sabbagh, M. Petkovski, K. Pilakoutas, R. Mirghaderi (2011). Ductile moment-resisting frames using cold-formed steel sections: An analytical investigation. Journal of Constructional Steel Research, 634–646.

[9] A. Bagheri Sabbagh, M. Petkovski, K. Pilakoutas, R. Mirghaderi (2012). Development of cold-formed steel elements for earthquake resistant moment frame buildings. Thin-Walled Structures, 53, 99–108.

[10] A. Bagheri Sabbagh, M. Petkovski, K. Pilakoutas, R. Mirghaderi (2012). Experimental work on cold-formed steel elements for earthquake resilient moment frame buildings. Engineering Structures, 42, 371–386.

[11] A. Bagheri Sabbagh, M. Petkovski, K. Pilakoutas, R. Mirghaderi (2013). Cyclic behaviour of bolted cold-formed steel moment connections: FEM including slip, Journal of Constructional Steel Research, 80, 100–108.

[12] Eurocode 8: Design of structures for earthquake resistance. Part 1, General rules, seismic actions and rules for buildings. BS EN 1998-1: 2004

[13] ANSI/AISC 341-05, 2005, Seismic Provisions for Structural Steel Buildings, American Institute of Steel Construction (AISC), Illinois

[14] M. Shahini, A. Bagheri Sabbagh, P. Davidson, R. Mirghaderi (2018). Improving Inelastic Capacity of Cold-Formed Steel Beams Using Slotted Blotted Connection, International Specialty Conference on Cold-Formed Steel Structures, CCFSS 2018 (St. Louis, Missouri), USA.

[15] M. Shahini, A. Bagheri Sabbagh, P. Davidson, R. Mirghaderi (2019). Development of cold-formed steel moment-resisting connections with bolting friction-slip mechanism for seismic applications. Thin-Walled Structures, 141, 217-231.

[16] B. Xu, D.V. Bompa, A.Y. Elghazouli (2020). Cyclic stress–strain rate-dependent response of rubberised concrete, Construction and Building Materials, 254, 119253.

[17] H-T. Thai, B. Uy, M. Khan, Z. Tao, F. Mashiri (2014). Numerical modelling of concrete-filled steel box columns incorporating high strength materials. Journal of Constructional Steel Research, 102 256–265.

[18] Li Z, Schafer BW (2010) “Buckling analysis of cold-formed steel members with general boundary conditions using CUFSM: conventional and constrained finite strip methods.” Proceedings of the 20th International Speciality Conference on Cold-Formed Steel Structures, St. Louis, MO.

[19] AISI-S100-16. North American Specification for the Design of Cold-Formed Steel Structural Members. Washington, D.C.: American Iron and Steel Institute; 2016.

[20] F. Tao, A. Chatterjee, C. D. Moen (2016). Monotonic and Cyclic Response of Single Shear Cold-Formed Steel-to-Steel and Sheathing-to-Steel Connections. Virginia Tech Report No. CE/VPI-ST-16-01

[21] Abaqus Analysis User's Manual, (2019). version 6.21.

[22] A. Bagheri Sabbagh, N. Jafarifar, P. Davidson, K. Ibrahimov (2022). Experiments on Cold-Formed Steel-Rubberised Concrete Semi-Rigid Moment-Resisting Connections. Under review.

[23] Eurocode 3: Design of steel structures: Part 1.8: Design of joints, BS-EN 1993-1-8; 2005.